Biogeosciences Discuss., doi:10.5194/bg-2016-142, 2016
Manuscript under review for journal Biogeosciences
Published: 25 April 2016

Manuscript for Biogeosciences

Title: Evaluation of modeled global carbon dynamics: analysis based on global carbon flux and above-ground biomass data

Running Title: Evaluation of modeled global carbon dynamics

Bao-Lin Xue[1], Qinghua Guo[1, 2,*], Tianyu Hu[1], Yongcai Wang[1], Shengli Tao[1], Yanjun Su[2], Jin Liu[1] and Xiaoqian Zhao[1]

[1]State Key Laboratory of Vegetation and Environmental Change, Institute of Botany, Chinese Academy of Sciences, No. 20 Nanxincun, Xiangshan, Beijing 100093, China

[2]School of Engineering, Sierra Nevada Research Institute, University of California at Merced, CA 95343, USA

Author Agreement:

All authors agree on the authorship of the manuscript and approve the submission.

***Corresponding author:**

Qinghua Guo, Dr., Prof.

State Key Laboratory of Vegetation and Environmental Change, Institute of Botany, Chinese Academy of Sciences, No. 20 Nanxincun, Xiangshan, Beijing 100093, China

Tel.: +86-10-6283-6473

Email: guo.qinghua@gmail.com

Biogeosciences Discuss., doi:10.5194/bg-2016-142, 2016
Manuscript under review for journal Biogeosciences
Published: 25 April 2016

Abstract

Dynamic global vegetation models are useful tools for the simulation of carbon dynamics on regional and global scales. However, even the most validated models are usually hampered by the poor availability of global biomass data in the model validation, especially on regional/global scales. Here, taking the integrated biosphere simulator model (IBIS) as an example, we evaluated the modeled carbon dynamics, including gross primary production (GPP) and potential above-ground biomass (AGB), on the global scale. The IBIS model was constrained by both in situ GPP and plot-level AGB data collected from the literature. Independent validation showed that IBIS could reproduce GPP and evapotranspiration with acceptable accuracy at site and global levels. On the global scale, the IBIS-simulated total AGB was similar to those obtained in other studies. However, discrepancies were observed between the model-derived and observed spatial patterns of AGB for Amazonian forests. The differences among the AGB spatial patterns were mainly caused by the single-parameter set of the model used. This study showed that different meteorological inputs can also introduce substantial differences in AGB on the global scale. Further analysis showed that this difference is small compared with parameter-induced differences. The conclusions of our research highlight the necessity of considering the heterogeneity of key model physiological parameters in modeling global AGB. The research also shows that to simulate large-scale carbon dynamics, both carbon flux and AGB data are necessary to constrain the model. The

main conclusions of our research will help to improve model simulations of global carbon cycles.

Keywords: dynamic global vegetation model, integrated biosphere model, gross primary production, above-ground biomass, global carbon cycle

Biogeosciences Discuss., doi:10.5194/bg-2016-142, 2016
Manuscript under review for journal Biogeosciences
Published: 25 April 2016

1 Introduction

The global terrestrial ecosystem is an important carbon sink that can mitigate the ongoing increases in atmospheric CO_2 concentration (Dixon et al., 1994; Luyssaert et al., 2007; Pan et al., 2011). For example, global forests, which cover around 30% of the land surface, account for ~75% of terrestrial gross primary production (GPP) and ~80% of global plant biomass (Kindermann et al., 2008; Beer et al., 2010). The large carbon stock in the terrestrial ecosystem indicates the need for a reliable description of its current distribution and prediction of future variations (Keith et al., 2009; Galbraith et al., 2010; Pan et al., 2011; Xue et al., 2011). However, it is still a challenge to accurately estimate the distribution of carbon stocks on the global scale, mainly because of the unknown mechanisms and/or relative contributions of various factors such as climate change, CO_2 fertilization, and land use change on carbon dynamics (McGuire et al., 2001; Mu et al., 2008).

Various methods have been developed for mapping the global distribution of biomass, and each has its pros and cons. On the regional scale, the field inventory method provides the most reliable information on biomass, but it is labor intensive and costly when applied over a large area (e.g., Malhi et al., 2002). On the global scale, remote-sensing methods have advantages over field inventory methods for applications to large areas and in areas that are difficult to access (Lefsky et al., 2005; Thurner et al., 2014; Tao et al., 2014). For example, the light detection and ranging method has recently been used in the Amazon region, with acceptable accuracy

(Asner et al., 2010; Saatchi et al., 2011). As an alternative, the dynamic global vegetation model (DGVM) is a useful tool for mapping global biomass and is the only method that predicts future variations. In the past, many researchers have explored how climate change or land use change would alter the global biomass, and this has improved our confidence in the projection of terrestrial responses to climate change. In many cases, the DGVM-modeled potential vegetation biomass is used as a baseline for exploring the corresponding response to the projected climate. Before using the DGVM to project future biomass changes, an evaluation of how the DGVM can reproduce potential (natural) present-day biomass is necessary (Mu et al., 2008; Seiler et al., 2014). However, this is rarely done, mainly because of the lack of available global-scale biomass data. For instance, in many cases, the default values for various physiological parameters are used, and may differ greatly for different DGVMs. The lack of evaluation of modeled biomass on the global scale may result in large differences among global carbon stocks obtained using different models (Cramer et al., 2001; Sitch et al., 2008), resulting in bias in our conclusions regarding vegetation responses in projected climate scenarios (Huntingford et al., 2008; 2013).

Uncertainty in the modeled biomass may originate in various ways: model structure, model parameters, and meteorological inputs. The results for potential natural vegetation obtained from bioclimatic limits and forest dynamics using the DGVM may give an unrealistic representation of competition among plant functional types (PFTs) (Purves and Pacala, 2008; Seiler et al., 2014). A biased PFT in the DGVM partly contributes to the uncertainty in carbon dynamics, including GPP and

Biogeosciences Discuss., doi:10.5194/bg-2016-142, 2016
Manuscript under review for journal Biogeosciences
Published: 25 April 2016

biomass. Moreover, DGVMs usually use a single set of parameters to represent different biomes and rarely consider spatial heterogeneity (Xiao et al., 2011, 2014). In reality, different physiological parameters vary greatly, depending on the soil type, climate, and vegetation (Castanho et al., 2013). The ways in which this will bias the spatial pattern of carbon flux, and thus biomass accumulation, have not been sufficiently discussed on the global scale, partly because of the unavailability of biomass data for large areas (Delbart et al., 2010; Wolf et al., 2011). Recent research has shown that it is necessary to use both carbon flux data and biometric data for DGVM calibration (Kondo et al., 2013; Seiler et al., 2014). Furthermore, uncertainties in DGVM-derived carbon flux and biomass may also arise from the input data itself, such as meteorological forcing data (Barman et al., 2014a, b). Different input data can result in differences among the results obtained using different models when modeling large-scale carbon flux (Zhao et al., 2005; Jung et al., 2007). It is therefore necessary to quantify the uncertainty from meteorological inputs in modeled biomass, to improve the modeling results.

The objective of this study is to evaluate model-derived carbon flux and biomass on the global scale using collected carbon flux (GPP) and biomass datasets at the plot level. To do this, we used the integrated biosphere simulator (IBIS; Foley et al., 1995; Kucharik et al., 2000) as an example, and used both carbon flux and collected above-ground biomass (AGB) data (2101 plots) to constrain the model. We adopted the most important parameters from meta-analysis, calibration, or from the literature. We also investigated how different meteorological input data changed the modeling

Biogeosciences Discuss., doi:10.5194/bg-2016-142, 2016
Manuscript under review for journal Biogeosciences
Published: 25 April 2016

results. Overall, the intention of the current study was to explore the following questions. 1) How accurately can IBIS simulate GPP and AGB, and where does bias originate? 2) Can a single set of calibrated parameters accurately map the patterns of GPP and AGB? 3) What should modelers do to improve the modeling results?

2 Material and methods

2.1 IBIS model

The IBIS model considers the composition and structure of vegetation responses to environmental changes, within an integrated framework, to simulate land surface hydrothermal processes, biogeochemical cycles, and terrestrial vegetation dynamics. The model simulates the land surface processes for energy, water, and momentum exchange between soil, vegetation, and the atmosphere, using a land surface transfer scheme (LSX) (Thompson and Pollard, 1995a, b). In detail, two canopy layers, three snow layers, and six soil layers are considered in each grid unit. Evapotranspiration (ET) consists of three components, i.e., canopy transpiration, interception, and evaporation from the ground surface. Vegetation transpiration is calculated using a semi-mechanistic model of stomatal conductance (Ball et al., 1986), which is coupled with canopy carbon assimilation and water exchange between a leaf and the boundary layer to give

$$g_{s,h_2o} = \frac{mA_n}{C_s} h_s + b \qquad (1)$$

where A_n is the net photosynthesis rate at leaf level (μmol CO_2 m^{-2} s^{-1}), $g_{s,h2o}$ is the

Biogeosciences Discuss., doi:10.5194/bg-2016-142, 2016
Manuscript under review for journal Biogeosciences
Published: 25 April 2016

leaf-level stomatal conductance of water vapor (μmol H_2O m^{-2} s^{-1}), C_s is the CO_2 concentration (μmol μmol^{-1}) at the leaf surfaces, h_s is the relative humidity at the leaf surface (%), and m and b are empirical parameters.

IBIS represents natural vegetation using PFTs, based on the biomass and leaf area index. Overall, 12 PFTs are defined in IBIS, related to bioclimatic limits, and physiological, morphological, phenological, and life-history criteria governing competition for light and water (Alton, 2011). Different physiological parameters are set for each PFT to quantify factors such as the phenological performance or carbon assimilation and water consumption characteristics (Kucharik et al., 2000). As a result, the GPP, and thus the net primary production (NPP) and vegetation transpiration, are calculated separately for upper (trees) and lower (shrublands and grass) canopies as

$$NPP = (1-\eta)\int (A_g - R_{leaf} - R_{stem} - R_{root})dt \quad (2)$$

where A_g is the gross canopy production, η is the fraction of carbon lost by growth respiration (fixed value of 0.3), and R_{leaf}, R_{stem}, and R_{root} are leaf, stem, and root respiration, respectively.

The model allows for the coexistence of different PFTs in a single grid cell. However, a dynamic vegetation mechanism is used to simulate annual changes in vegetation structure through PFT competition for light, water, and other nutrient resource pools (Kucharik et al., 2006). The competition among PFTs is driven by differences among carbon balances resulting from phenology, leaf form, and photosynthetic pathways (Foley et al., 1996; Kucharik et al., 2000). On the annual scale, the NPP is allocated among three carbon pools, i.e., leaves, stems (for trees),

Biogeosciences Discuss., doi:10.5194/bg-2016-142, 2016
Manuscript under review for journal Biogeosciences
Published: 25 April 2016

and roots. The instantaneous change in the biomass pool *j* of PFT *i* is represented as

$$\frac{\partial C_{i,j}}{\partial t} = a_{i,j} NPP_i - \frac{C_{i,j}}{\tau_{i,j}} \quad (3)$$

where $a_{i,j}$ is the fraction of annual NPP allocated to the biomass pool and $\tau_{i,j}$ is the carbon residence time of that biomass pool. Note that $a_{i,j}$ is a fixed value in IBIS, but in some other DGVMs (e.g., the Lund–Potsdam–Jena dynamic global vegetation model, Sitch et al., 2003) the NPP is allocated using allometric equations.

A relatively simple phenology module based on accumulated growing degree days (Botta et al., 2000) is used in the original IBIS. A modified version of the phenology scheme, based on that reported by Jolly et al. (2005), was developed in this study. In detail, the prognostic phenology model is based on the growing season index (GSI), which is decided by three main environmental factors, i.e., temperature, photoperiod, and humidity (Equation 4). The photoperiod is calculated according to the latitude of the model grid and empirical algorithms. We also adopted a 21-day running mean GSI calculated from daily mean meteorological variables, following Jolly et al. (2005).

$$GSI = f(\overline{T_m}) \times f(\overline{R_g}) \times f(\overline{VPD}) \quad (4)$$

where T_m, R_g, and VPD are multi-day running mean averages of air temperature (℃), solar radiation (W m^{-2}) and vapor pressure deficit (Pa); $f(\overline{Tm})$, $f(\overline{Rg})$, and $f(\overline{VPD})$ vary linearly between the constraining limits 0 and 1, and thus regulate vegetation activity; these functions are defined in Equations (2–4) in Stöckli et al. (2008).

Biogeosciences Discuss., doi:10.5194/bg-2016-142, 2016
Manuscript under review for journal Biogeosciences
Published: 25 April 2016

2.2 Model input data

In the present study, IBIS was executed globally at a 0.5° × 0.5° latitude–longitude grid resolution. The initial vegetation type was obtained from moderate-resolution imaging spectoradiometer (MODIS) MOD12Q1 product (Friedl et al., 2010), and resampled to 0.5°. Soil texture data were obtained from the Center for Sustainability and the Global Environment (http://www.sage.wisc.edu/download/IBIS/ibis.html), and was reformatted from the Global Soil Data Products CD-ROM issued by the International Geosphere–Biosphere Programme Data and Information Services. The topographical data were obtained from the Shuttle Radar Topographic Mission (http://srtm.usgs.gov/), with a resolution of 1000 m. We resampled the resolution to 0.5°(~ 50 km) as a model grid.

The climate data, including monthly mean air temperature, precipitation, relative humidity, cloudiness, diurnal temperature range, wind speed, and the number of wet days, were obtained from the Climate Research Unit (CRU) climate dataset for 1901 through 2010 (CRUTS3.10, Harris et al. 2013, hereafter CRU). We examined the modeled biomass uncertainty induced by different meteorological datasets using forcing data from Princeton University (http://hydrology.princeton.edu/data.pgf.php, hereafter Princeton) to drive the model. Princeton does not include wind speed, therefore we use the wind speed data from the Global Land Data Assimilation System covering the period 1948–2010 (http://disc.sci.gsfc.nasa.gov/services/grads-gds/gldas). The Princeton was developed at a global spatial scale of 0.5°, with a daily timescale.

Biogeosciences Discuss., doi:10.5194/bg-2016-142, 2016
Manuscript under review for journal Biogeosciences
Published: 25 April 2016

In both cases, we spun-up the model for 400 years and then conducted transient simulations starting from 1948, and 1901 climate data were used for the years before 1901.

2.3 Model validation data

To calibrate and validate the IBIS model, we collected site-level GPP and ET data from Fluxnet (http://fluxnet.ornl.gov/). The validation sites and data were carefully selected; we only collected sites with at least 3 years' data, because there may be greater uncertainty for sites that cover only 1 or 2 years. Thirty-nine sites were selected, covering tropical, temperate, and boreal forests, and grasslands or croplands (Fig. S1, Table S1). Note that IBIS does not simulate croplands explicitly; therefore croplands were compared with the simulation results for the understory. The calibration and validation were conducted on both monthly and annul scales.

To constrain the model with both flux and biometric data, we also collected plot-level AGB data from the literature. Overall, 2101 site-year biomass data were obtained on the global scale (Fig. S1, Table S1). The resolution of plot-level data is usually 0.01°; therefore we used the average value as a proxy for a model grid. We also evaluated the modeled AGB on the regional scale. In detail, we first generated a regional AGB map for tropical Amazonian forests using collected plot data (~ 400 plots) by the random forest method (Breiman, 2001); the data were then resampled at 0.5° for comparison with the modeling results. Note that the model calculates the carbon density (Mg C ha^{-1}) instead of the AGB, therefore we calculated the AGB (Mg

ha^{-1}) by multiplying by a factor of 2.0 (IPCC, 2003).

3 Results

To minimize the number of parameters for calibration, we used most of the default values, as in Foley et al. (1996) and Kucharik et al. (2000); we calibrated the parameters most sensitive to the GPP and ET (Table 1). We mainly calibrated the photosynthesis capacity at 15 ℃ (vmax_pft) for different PFTs, as in Castanho et al. (2013). The flux data were mainly for boreal and temperate forests and grassland (including crops), because of the gaps in data for tropical forest. We therefore used the literature value for tropical forest (Zhu et al., 2011). Furthermore, we validated the GPP and ET on the annual scale globally, by comparison with other released datasets.

3.1 Monthly-scale calibrations

The model performs well for most sites after calibration (Table 2). The Taylor diagram shows a high correlation between the modeled and observed values for both GPP and ET (Fig. 1). Most sites have correlation coefficients above 0.6 for GPP and ET on the monthly scale. The model performance for ET is better than that for GPP, with large correlation coefficients and larger determination coefficients, averaged as 0.60 and 0.74, respectively, for 39 sites (Fig. 1 and Table 2). This shows that the model can simulate the energy balance well, according to the LSX land surface subsection. The model simulates upper canopy (forests) better than lower canopy (shrubs and grasses), with large correlation coefficients and small deviations from 1

Biogeosciences Discuss., doi:10.5194/bg-2016-142, 2016
Manuscript under review for journal Biogeosciences
Published: 25 April 2016

for the GPP slope (Fig. 1 and Table 2).

3.2 Annual-scale validations

We compared our simulated GPP and ET results with annual-scale in situ observations (Fig. 2). There are strong relationships between the model simulation and in situ values for both GPP and ET (R^2 = 0.57, p < 0.001 and R^2 = 0.64 p < 0.001 for GPP and ET, respectively). In both cases, the simulations slightly overestimate small values with large intercepts and slightly underestimate large values compared with the in situ observations. This overestimation of low values is clearly seen in independent validation by collected GPP from the literature (Fig. 2c). When the GPPs were below 500 gC m^{-2} year^{-1}, the simulated GPPs were around twice the observed values. This systematic error may be caused by differences between the flux tower fetch and the model grid resolution (Kim et al., 2006). Another reason may be that the flux tower generally focuses on high-production ecosystems (Turner et al., 2006).

3.3 Global annual-scale validations

We further validated the simulated annual GPP and ET results with those from Jung et al. (2011), on the global scale (Fig. 3). The GPP and ET were scaled up from flux tower values using the machine-learning technique reported in Jung et al. (2011), at the same resolution as our model grid (0.5° × 0.5°). The modeled global average GPP is 1112 gC m^{-2} year^{-1} for 2000–2010; this is larger than the value reported by Jung et al. (2011) (933 gC m^{-2} year^{-1}). The corresponding total global GPP during this period is 142 PgC year^{-1} for the model simulation. The modeled GPPs for Amazonian and African tropical areas are usually above 2800 gC m^{-2} year^{-1}, whereas the value for tropical forests in southeastern Asia are usually above 3200 gC m^{-2} year^{-1}. Our model simulation values are ~200 gC m^{-2} year^{-1} larger than those reported by Jung et al. (2011) for most areas, especially for areas with small GPPs (Fig. 3b). This difference is even larger in southern China and the southern US. In contrast, the GPP is less than that reported by Jung et al. (2011) for southern Amazonian areas.

Similar patterns to those for GPP are found for ET in the model simulations. The global average ET is 449 mm year^{-1}, compared with the value of 546 mm year^{-1} reported by Jung et al. (2011). In most areas, the model simulation results are around 100 mm year^{-1} smaller than those from Jung et al. (2011), especially for low ET areas (Fig. 4). However, the modeled ET is around 200 mm year^{-1} larger than that obtained by Jung et al. (2011) for Amazonian and southeastern Asian tropical areas (Fig. 4b).

3.4 Plot-level biomass calibrations

Fig. 5 shows a comparison of the modeled biomass with plot-level observations after calibration. Fig. 5a shows all the site-year data for each plot, and Fig. 5b shows the grid-averaged comparisons. The simulations show strong correlations in both cases. The regression is better for the grid-level case. The improved regression relationship in the grid-level comparison is caused by the scale difference between the site location (0.01°) and the model grid (0.5°). In both cases, the model overestimated low values but underestimated large ones. As stated in section 2.3, the plot accuracy is

Biogeosciences Discuss., doi:10.5194/bg-2016-142, 2016
Manuscript under review for journal Biogeosciences
Published: 25 April 2016

Biogeosciences Discussions

usually 0.01°, therefore the modeled values seem “saturated” in some cases, as observations vary if they are within the same grid. Fig. 5c shows an independent validation of the modeled biomass by plot-level observations. The plots are mainly from measured AGB from natural forests in China. The regression relationship is significant, but also has large scattering in the calibration. Overall, the model seems to underestimate large values, but overestimate small values (below 50 Mg ha^{-1}).

3.5 Global and regional AGBs

Fig. 6a shows the spatial pattern of the model-derived above-ground global biomass (upper and under layers). The global average biomass is 81.73 Mg ha^{-1}, with the largest values in tropical areas and the lowest in boreal areas. The global map of AGB shows large heterogeneity, which is similar to the case for global GPP patterns. The zonal AGB within each 0.5° latitude interval shows a large fluctuation (Fig. 6b). The AGB is relatively small below −30° S and then starts to increase sharply to a maximum of 278.44 Mg ha^{-1} at around −1.25° S (AGB = 10.814 × latitude + 291.03, R^2 = 0.95, $p < 0.001$). The AGB then decreases sharply until 13.75° N (AGB = −8.04 × latitude + 313.3, R^2 = 0.95, $p < 0.001$). The AGB is relatively constant between 15° N and 50° N and then increases. The AGB reaches another maximum, 112.17 Mg ha^{-1}, at around 56.25° N, and decreases continuously to close to 0 at around 75° N.

Fig. 7 shows a comparison of the regional AGBs for Amazonian tropical forests. The observed regional AGBs are derived from 399 plot-level data using a random forest method. The calculated average AGB is 280.27 Mg ha^{-1}, and shows a

Biogeosciences Discuss., doi:10.5194/bg-2016-142, 2016
Manuscript under review for journal Biogeosciences
Published: 25 April 2016

decreasing gradient from east to west. The model calculates the average AGB in this area as 285.95 Mg ha^{-1}, which is comparable to the observed value. However, our modeled AGB does not show a decreasing gradient from east to west, but shows a decreasing gradient from north to south gradient as that for GPP (Fig. 6). The model therefore underestimates the large AGB in the east and overestimates the AGB in the west (Fig. 7b). Most grids in the Amazonian region are within a ±30% relative error [(Model − Observation)/Observation × 100%) (Fig. 7b). This results in a small absolute error of 4.42 Mg ha^{-1} over the whole area.

3.6 Global AGB driven by CRU metrological data

Fig. 8 shows the spatial pattern of the difference between AGBs driven by Princeton and CRU. Most areas of the globe show AGB differences within 20 Mg ha^{-1}, according to the two meteorological datasets. The average global difference is 12.83 Mg ha^{-1}, with large heterogeneities in different areas. Large differences are observed in savanna regions (MODIS UMD classification scheme) in South America and central Africa, and shrublands in northeastern Siberia (Fig. 8a). In these areas, the AGB driven by daily meteorological data (Princeton) is significantly larger than those derived from CRU data. In contrast, in most tropical areas, the AGB derived from Princeton datasets is smaller than those derived from CRU datasets. Most of the grids show a relative error within ±20% with largest frequency occurs for relative error of 10 % (Fig. 8b).

Biogeosciences Discuss., doi:10.5194/bg-2016-142, 2016
Manuscript under review for journal Biogeosciences
Published: 25 April 2016

4 Discussion

We used a single set of model parameters to estimate the global carbon stock in terms of AGB. The IBIS model does not calculate the global AGB directly, but calculates the carbon density. We therefore compared our model-derived carbon density with those from other studies. Comparisons of carbon densities have the advantage over AGB comparisons that they eliminate the uncertainties induced by global vegetation areas used in different studies. Our model-derived carbon density is smaller than that reported by Pan et al. (2011) on the global scale (82.96 compared with 94.2 Mg C ha^{-1}), and this results in a smaller global carbon stock (Table 3). Pan et al. (2011) calculated the carbon density, using the forest inventory method, for the period 1990–2007; their estimated value of 94.2 Mg C ha^{-1} includes both above- and below-ground biomass. Previous research showed that ~80% of the total biomass is in AGB and ~20% is in below-ground biomass for forest ecosystems on the global scale (Cairns et al., 1997). This indicates that the global above-ground carbon density is ~75 Mg C ha^{-1} for Pan et al. (2011). This value is comparable to our modeling result. The difference between the global carbon stocks in AGB may arise from the different forest areas used by Pan et al. (2011) and in our study (MODIS derived). The forest areas were 3851.3 × 10^{6} and 3332.35 × 10^{6} ha in Pan et al.'s study and our study, respectively. Further comparison of the regional-scale carbon density with those from three other studies show that values in our study and those reported by Pan et al. (2011) are larger. The carbon densities reported by Goodale et al. (2002) and Liski et al. (2003) are around 30% smaller than those reported by Thurner et al. (2014) and in our study for European forests. In contrast, for North American forests, the carbon densities reported by Pan et al. (2011) and in our study are similar, and larger than those in the other three studies. These comparisons with other studies show that the IBIS-model-derived carbon density gives reasonable results on the global scale and can therefore be used as an independent tool for validating AGB estimations by other methods.

A regional-scale comparison of the observed and modeled AGBs for Amazonian tropical forests shows that the spatial patterns in the modeling results are biased (Fig. 7). The relative error between the modeled and observed GPPs in this region is usually below 10% (Figs. 2 and 3). However, the relative error in the AGB for most grids is within ±30% (Fig. 7). This indicates that the uncertainty in the modeled AGB may be mainly caused by woody carbon residence (τ_w, Table 1) instead of carbon assimilation. Though our point-level calibration shows a significant relationship between modeled and plot level data, the calibration points are subject to scatter. Independent validation shows that the model tends to underestimate the AGB when the AGB is large (Fig. 5c). Similar determination coefficients (R^2) were reported by Seiler et al. (2013) for a regional-scale model calibration in Bolivia. The relatively small R^2 may explain the region-scale difference for Amazonian forests. The single value of τ_w in the model cannot reproduce the spatial variance of AGB on a large scale. Similar research by Castanho et al. (2013) showed that the woody biomass residence time is the most important parameter in determining the spatial variance in modeled AGB in this area. Further investigation using a spatial pattern of τ_w in IBIS greatly improved the modeled AGB, with R^2 changing from 0.33 to 0.88 (Castanho et al., 2013). These and the presented results indicate that to improve the model simulation accuracy, modelers should consider the spatial heterogeneity of the most important parameters in the model used, especially for large-scale simulations (e.g., Zhou et al., 2009).

Climate-data-driven uncertainties in modeling carbon and energy cycles have previously been analyzed (Zhao et al., 2005; Barman et al., 2014a, b). A systematic analysis based on various global vegetation models and meteorological data showed that substantial changes in the modeled GPP were observed for different meteorological inputs in regional simulations in Europe (Jung et al., 2007). The interannual variations in the GPP were mainly caused by different meteorological drivers. A similar analysis by Barman et al. (2014b) showed that the differences in site-level GPPs caused by different meteorological drivers were ~20% of the annual GPP. This was mainly caused by biases in short-wave radiation and humidity for various meteorological drivers tested in the study. Our study results show that climate-data-driven uncertainties in carbon assimilation (GPP) can be transferred to the AGB carbon stock (Fig. 8). The relative differences caused by different climate drivers are generally within ±20% (Fig. 8b). These differences are smaller than the relative errors induced by the invariant parameters over the Amazonian forest. This indicates that to improve the model simulation accuracy, modelers should pay attention to both model parameter calibration and metrological drivers, with a focus on the former.

Data availability is one of the main reasons that few global model simulations use plot-level data to constrain the model (Seiler et al., 2014). We collected plot-level AGB data from the literature, and used them to calibrate and validate IBIS on the global scale. The plot resolution was generally 0.01–0.1° (~1–10 km). In the validation, we used measured single-point values as a proxy for a model grid average (~2500 km^2), which may have caused a bias relative to the modeled values. Note that even over a small area, AGB may vary greatly because of local soil type, land use variability, and local water availability (Baker et al., 2004). Therefore, the difference between the spatial scales of the plot level and our model simulation grid may partly explain the small R^2 in Fig. 5. Further investigations of model simulations at different spatial resolution (especially at high resolution) are therefore necessary to facilitate model calibration by higher spatial resolution AGB datasets. Furthermore, the plot points used for validation and calibration are from natural forests, with little human disturbance, therefore our modeling results represent the potential value under current climate conditions (e.g., Mu et al., 2008; Seiler et al., 2014). The AGBs in Table 2 are present-day AGBs, which may be influenced by human activities. A direct comparison of model simulation and these data is therefore to some extent inappropriate. However, this comparison is useful, because based on exploration of the difference between the two, the model could be used to quantify the impact of human activities (such as land use change, deforestation, or afforestation) on large-scale AGB change.

5 Conclusions

DGVMs are useful tools for simulation of regional- and global-scale carbon

Biogeosciences Discuss., doi:10.5194/bg-2016-142, 2016
Manuscript under review for journal Biogeosciences
Published: 25 April 2016

dynamics. In this research, we evaluated the model performance in modeling global carbon dynamics after calibration of IBIS using in situ GPP and plot-level AGB data collected from the literature. Independent validation showed that IBIS can reproduce GPP and ET with acceptable accuracies at the site and global levels. On the global-scale, IBIS simulation of total AGB gave results similar to those obtained in other studies. However, discrepancies were observed between model-derived and observed spatial patterns of AGB for Amazonian forests, mainly because of the unique parameter set used in the model. Two metrological datasets, i.e., Princeton and CRU, were used to test the model uncertainties caused by climate drivers. The results indicated that the two meteorological inputs give substantially different global-scale AGBs. Further analysis showed that this difference was small compared with the parameter-induced difference. The conclusions of our research highlight the necessity of considering the heterogeneity of key model physiological parameters in modeling global AGB. The research also shows that to simulate large-scale carbon dynamics, both carbon flux and AGB data are necessary to constrain the model. The main conclusions of our research could help to improve model simulation of the global carbon cycle.

Acknowledgements

This study was financially supported by the National Science Foundation of China (Grant No. 41301020) and the National Key Basic Research Program of China (2013CB956604). We are grateful to the PIs and Co-Is of FLUXNET who make their data freely available to the ecological modelling community through the FLUXNET

Biogeosciences Discuss., doi:10.5194/bg-2016-142, 2016
Manuscript under review for journal Biogeosciences
Published: 25 April 2016

archive (http://fluxnet.ornl.gov/), in particular by the following networks: AmeriFlux (U.S. Department of Energy, Biological and Environmental Research, Terrestrial Carbon Program (DE-FG02-04ER63917 and DE-FG02-04ER63911)), AfriFlux, AsiaFlux, CarboAfrica, CarboEuropeIP, CarboItaly, CarboMont, ChinaFlux, Fluxnet-Canada (supported by CFCAS, NSERC, BIOCAP, Environment Canada, and NRCan), GreenGrass, KoFlux, LBA, NECC, OzFlux, TCOS-Siberia, USCCC. We acknowledge the financial support to the eddy covariance data harmonization provided by CarboEuropeIP, FAO-GTOS-TCO, iLEAPS, Max Planck Institute for Biogeochemistry, National Science Foundation, University of Tuscia, Université Laval, Environment Canada and US Department of Energy and the database development and technical support from Berkeley Water Center, Lawrence Berkeley National Laboratory, Microsoft Research eScience, Oak Ridge National Laboratory, University of California – Berkeley and the University of Virginia.

References

Alton, P.B., 2011. How useful are plant functional types in global simulations of the carbon, water, and energy cycles? Journal of Geophysical Research – Biogeosciences, 116.

Asner, G.P. et al., 2010. High-resolution forest carbon stocks and emissions in the Amazon. Proceedings of the National Academy of Sciences of the United States of America, 107(38), 16738–16742.

Baker, T.R. et al., 2004. Variation in wood density determines spatial patterns in Amazonian forest biomass. Global Change Biology, 10(5), 545–562.

Ball J.T., Woodrow I.E., and Berry J.A., 1987. A model predicting stomatal conductance and its contribution to the control of photosynthesis under different environmental conditions. In Progress in Photosynthesis Research, Biggens J (ed.), pp. 221–224. Springer: New York.

Barman, R., Jain, A.K. and Liang, M., 2014a. Climate-driven uncertainties in modeling terrestrial energy and water fluxes: a site-level to global-scale analysis. Global Change Biology, 20(6), 1885–1900.

Barman, R., Jain, A.K. and Liang, M., 2014b. Climate-driven uncertainties in modeling terrestrial gross primary production: a site level to global-scale analysis. Global Change Biology, 20(5), 1394–1411.

Beer, C. et al., 2010. Terrestrial gross carbon dioxide uptake: global distribution and covariation with climate. Science, 329(5993), 834–838.

Botta, A., Viovy, N., Ciais, P., Friedlingstein, P. and Monfray, P., 2000. A global prognostic scheme of leaf onset using satellite data. Global Change Biology, 6(7), 709–725.

Breiman, L., 2001. Random forests. Machine Learning, 45(1), 5–32.

Cairns, M.A., Brown, S., Helmer, E.H. and Baumgardner, G.A., 1997. Root biomass allocation in the world's upland forests. Oecologia, 111(1), 1–11.

Castanho, A.D.A. et al., 2013. Improving simulated Amazon forest biomass and productivity by including spatial variation in biophysical parameters. Biogeosciences, 10(4), 2255–2272.

Cox, P.M. et al., 2008. Increasing risk of Amazonian drought due to decreasing aerosol pollution. Nature, 453(7192), 212–U7.

Cramer, W. et al., 2001. Global response of terrestrial ecosystem structure and function to CO_2 and climate change: results from six dynamic global vegetation models. Global Change Biology, 7(4), 357–373.

Delbart, N. et al., 2010. Mortality as a key driver of the spatial distribution of aboveground biomass in Amazonian forest: results from a dynamic vegetation model. Biogeosciences, 7(10), 3027–3039.

Dixon, R.K. et al., 1994. Carbon pools and flux of global forest ecosystems. Science, 263(5144), 185–190.

Friedl, M.A. et al., 2010. MODIS Collection 5 global land cover: Algorithm refinements and characterization of new datasets. Remote Sensing of

Environment 114: 168-182.

Foley, J.A. et al., 1996. An integrated biosphere model of land surface processes, terrestrial carbon balance, and vegetation dynamics. Global Biogeochemical Cycles, 10(4), 603–628.

Galbraith, D. et al., 2010. Multiple mechanisms of Amazonian forest biomass losses in three dynamic global vegetation models under climate change. New Phytologist, 187(3), 647–665.

Goodale, C.L. et al., 2002. Forest carbon sinks in the Northern Hemisphere. Ecological Applications, 12(3), 891–899.

Harris, I., Jones, P.D., Osborn, T.J. and Lister, D.H., 2014. Updated high-resolution grids of monthly climatic observations – the CRU TS3.10 Dataset. International Journal of Climatology, 34(3), 623–642.

Houghton, R.A., 2005. Aboveground forest biomass and the global carbon balance. Global Change Biology, 11(6), 945–958.

Huntingford, C. et al., 2008. Towards quantifying uncertainty in predictions of Amazon 'dieback'. Philosophical Transactions of the Royal Society B – Biological Sciences, 363(1498), 1857–1864.

Huntingford, C. et al., 2013. Simulated resilience of tropical rainforests to CO_2-induced climate change. Nature Geoscience, 6(4), 268–273.

IPCC (Intergovernmental Panel on Climate Change), 2003. Good practice guidance for land use, land-use change and forestry (ed. J. Penman, M. Gytarsky, T. Hiraishi, T. Krug, D. Kruger, R. Pipatti, L. Buendia, K. Miwa, T. Ngara, K. Tanabeand, and F. Wagner), pp. 3.14–G.9. Institute for Global Environmental Strategies: Kanagawa, Japan.

Jolly, W.M., Nemani, R. and Running, S.W., 2005. A generalized, bioclimatic index to predict foliar phenology in response to climate. Global Change Biology, 11(4), 619–632.

Jung, M. et al., 2011. Global patterns of land-atmosphere fluxes of carbon dioxide, latent heat, and sensible heat derived from eddy covariance, satellite, and meteorological observations. Journal of Geophysical Research – Biogeosciences, 116.

Keith, H., Mackey, B.G. and Lindenmayer, D.B., 2009. Re-evaluation of forest biomass carbon stocks and lessons from the world's most carbon-dense forests. Proceedings of the National Academy of Sciences of the United States of America, 106(28), 11635–11640.

Kindermann, G. et al., 2008. Global cost estimates of reducing carbon emissions through avoided deforestation. Proceedings of the National Academy of Sciences of the United States of America, 105(30), 10302–10307.

Kondo, M. et al., 2013. The role of carbon flux and biometric observations in constraining a terrestrial ecosystem model: a case study in disturbed forests in East Asia. Ecological Research, 28(5), 893–905.

Kucharik, C.J. et al., 2006. A multiyear evaluation of a Dynamic Global Vegetation Model at three AmeriFlux forest sites: Vegetation structure, phenology, soil temperature, and CO_2 and H_2O vapor exchange. Ecological Modelling, 196(1–2), 1–31.

Kucharik, C.J. et al., 2000. Testing the performance of a Dynamic Global Ecosystem Model: Water balance, carbon balance, and vegetation structure. Global Biogeochemical Cycles, 14(3), 795–825.

Lefsky, M.A. et al., 2005. Estimates of forest canopy height and aboveground biomass using ICESat. Geophysical Research Letters, 32(22).

Liski, J. et al., 2003. Increased carbon sink in temperate and boreal forests. Climatic Change, 61(1–2), 89–99.

Liu, D. et al., 2014. The contribution of China's Grain to Green Program to carbon sequestration. Landscape Ecology, 29(10), 1675–1688.

Luyssaert, S. et al., 2007. CO_2 balance of boreal, temperate, and tropical forests derived from a global database. Global Change Biology, 13(12), 2509–2537.

Malhi, Y. et al., 2002. An international network to monitor the structure, composition and dynamics of Amazonian forests (RAINFOR). Journal of Vegetation Science, 13(3), 439–450.

McGuire, A.D. et al., 2001. Carbon balance of the terrestrial biosphere in the twentieth century: Analyses of CO_2, climate and land use effects with four process-based ecosystem models. Global Biogeochemical Cycles, 15(1), 183–206.

Mu, Q., Zhao, M., Running, S.W., Liu, M. and Tian, H., 2008. Contribution of increasing CO_2 and climate change to the carbon cycle in China's ecosystems. Journal of Geophysical Research – Biogeosciences, 113(G1).

Pan, Y. et al., 2011. A large and persistent carbon sink in the world's forests. Science, 333(6045), 988–993.

Pan, Y., Birdsey, R.A., Phillips, O.L. and Jackson, R.B., 2013. The structure, distribution, and biomass of the world's forests. Annual Review of Ecology, Evolution, and Systematics, Vol 44, 44, 593-622.

Purves, D. and Pacala, S., 2008. Predictive models of forest dynamics. Science, 320(5882), 1452–1453.

Saatchi, S.S. et al., 2011. Benchmark map of forest carbon stocks in tropical regions across three continents. Proceedings of the National Academy of Sciences of the United States of America, 108(24), 9899–9904.

Seiler, C. et al., 2014. Modeling forest dynamics along climate gradients in Bolivia. Journal of Geophysical Research – Biogeosciences, 119(5), 758–775.

Sitch, S. et al., 2008. Evaluation of the terrestrial carbon cycle, future plant geography and climate-carbon cycle feedbacks using five Dynamic Global Vegetation Models (DGVMs). Global Change Biology, 14(9), 2015–2039.

Sitch, S. et al., 2003. Evaluation of ecosystem dynamics, plant geography and terrestrial carbon cycling in the LPJ dynamic global vegetation model. Global Change Biology, 9(2), 161–185.

Tao, S. et al., 2014. Airborne Lidar-derived volume metrics for aboveground biomass estimation: A comparative assessment for conifer stands. Agricultural and Forest Meteorology, 198, 24–32.

Thompson, S.L. and Pollard, D., 1995a. A global climate model (genesis) with a

Biogeosciences Discuss., doi:10.5194/bg-2016-142, 2016
Manuscript under review for journal Biogeosciences
Published: 25 April 2016

land-surface transfer scheme (LSX). 1. Present climate simulation. Journal of Climate, 8(4), 732–761.

Thompson, S.L. and Pollard, D., 1995b. A global climate model (genesis) with a land-surface transfer scheme (LSX). 2. CO_2 sensitivity. Journal of Climate, 8(5), 1104–1121.

Thurner, M. et al., 2014. Carbon stock and density of northern boreal and temperate forests. Global Ecology and Biogeography, 23(3), 297–310.

Wolf, A. et al., 2011. Forest biomass allometry in global land surface models. Global Biogeochemical Cycles, 25.

Xiao, J., Davis, K.J., Urban, N.M. and Keller, K., 2014. Uncertainty in model parameters and regional carbon fluxes: A model-data fusion approach. Agricultural and Forest Meteorology, 189, 175–186.

Xiao, J., Davis, K.J., Urban, N.M., Keller, K. and Saliendra, N.Z., 2011. Upscaling carbon fluxes from towers to the regional scale: Influence of parameter variability and land cover representation on regional flux estimates. Journal of Geophysical Research – Biogeosciences, 116.

Xue, B.-L. et al., 2011. Influences of canopy structure and physiological traits on flux partitioning between understory and overstory in an eastern Siberian boreal larch forest. Ecological Modelling, 222(8), 1479-1490.

Zhao, M.S., Heinsch, F.A., Nemani, R.R. and Running, S.W., 2005. Improvements of the MODIS terrestrial gross and net primary production global data set. Remote Sensing of Environment, 95(2), 164–176.

Zhu, Q. et al., 2011. Evaluating the effects of future climate change and elevated CO_2 on the water use efficiency in terrestrial ecosystems of China. Ecological Modelling, 222(14), 2414–2429.

Biogeosciences Discuss., doi:10.5194/bg-2016-142, 2016
Manuscript under review for journal Biogeosciences
Published: 25 April 2016

Tables

Table 1 Key PFT-dependent parameters for IBIS calibration. The abbreviations are defined as follows: vmax_pft: maximum Rubisco capacity at top of canopy (μmol m^{-2} s^{-1}); SLA: specific leaf area (m^2 kg^{-1}); τ_l: residence time of foliar biomass (years); τ_r: residence time of root biomass (years); τ_w: residence time of wood biomass (years); a_{leaf}: allocation coefficient of total photosynthate in foliar biomass (fraction); a_{root}: allocation coefficient of total photosynthate in root biomass (fraction); a_{wood}: allocation coefficient of total photosynthate in wood biomass (fraction); P_{min}: monthly minimum precipitation (mm $month^{-1}$); T_{minL}: absolute minimum temperature (lower limit, ℃); T_{minU}: absolute minimum temperature (upper limit, ℃); T_{warm}: temperature of the warmest month (℃) (C_4 plants only); GDD: minimum growing degree days above 5 ℃ threshold for upper-canopy types; minimum growing degree days above 0 ℃ threshold for lower-canopy types. The plant functional type (PFT) numbers defined in IBIS are as follows: 1, tropical broadleaf evergreen trees; 2, tropical broadleaf drought-deciduous trees; 3, warm–temperate broadleaf evergreen trees; 4, temperate conifer evergreen trees; 5, temperate broadleaf cold-deciduous trees; 6, boreal conifer evergreen trees; 7, boreal broadleaf cold-deciduous trees; 8, boreal conifer cold-deciduous trees; 9, evergreen shrubs; 10: cold-deciduous shrubs; 11, warm (C4) grasses; and 12, cool (C3) grasses.

PFT	*vmax_pft*	*SLA*	τ_l	τ_r	τ_w	a_{leaf}	a_{root}	a_{wood}	P_{min}	T_{minL}	T_{minU}	T_{warm}	*GDD*
1	55	25	1.01	1	60	0.3	0.3	0.4	>5.0	>0.0	–	–	–
2	45	25	1	1	60	0.3	0.3	0.4	–	>0.0	–	–	–
3	40	25	1	1	25	0.3	0.3	0.4	–	>−5.0	<0.0	–	–
4	30	12.5	2	1	35	0.3	0.4	0.3	–	>−45.0	<0.0	–	>1100
5	40	25	1	1	35	0.3	0.3	0.4	–	>−45.0	<0.0	–	>1100
6	25	12.5	2.5	1	52	0.3	0.4	0.3	–	>−57.5	<−45.0	–	>350
7	30	25	1	1	52	0.3	0.3	0.4	–	>−57.5	<−45.0	–	>350
8	35	25	1	1	52	0.3	0.3	0.4	–	–	<−45.0	–	>350
9	27.5	12.5	1.5	1	5	0.45	0.4	0.15	–	–	–	–	>100
10	27.5	25	1	1	5	0.45	0.35	0.2	–	–	–	–	>100
11	15	20	1.25	1	–	0.45	0.55	0	–	–	–	>22.0	>100
12	25	20	1.5	1	–	0.45	0.55	0	–	–	–	–	>100

Table 2 Comparison of observed and model-derived gross primary production (GPP; gC m^{-2} month^{-1}) and evapotranspiration (ET; mm month^{-1}) for 39 sites. The regression coefficients of slope (*a*), intercept (*b*), R^2, and root-mean-square error (RMSE) deviations are also shown. The PFT definitions are the same as in Table 1.

Longitude	Latitude	Site	PFT	GPP (gC m^{-2} month^{-1})				ET (mm m^{-2} month^{-1})			
				a	*b*	R^2	RMSE	*a*	*b*	R^2	RMSE
131.15	-12.49	Au-How	2	1.54	-64.90	0.73	50.13	1.06	-37.31	0.54	39.18
-68.75	45.21	US-Ho2	4	1.11	-2.42	0.97	18.95	0.99	8.40	0.93	8.61
-121.56	44.45	US-Me2	4	0.74	6.91	0.93	16.44	0.56	5.56	0.67	10.68
-121.61	44.32	US-Me3	4	1.14	14.96	0.91	18.20	0.72	9.19	0.71	10.22
-121.57	44.44	US-Me5	4	1.18	12.55	0.90	18.43	0.72	7.10	0.73	9.13
-76.67	35.80	US-NC2	4	0.64	62.28	0.85	25.13	0.78	-1.89	0.92	9.81
-105.55	40.03	US-NR1	4	0.53	11.09	0.70	22.29	0.52	4.65	0.59	11.75
-89.87	34.25	US-Goo	5	0.54	128.53	0.48	53.27	0.69	19.37	0.65	18.71
-72.17	42.54	US-Ha1	5	0.65	67.39	0.69	59.59	0.86	12.60	0.86	11.72
-72.19	42.54	US-LPH	5	0.56	82.25	0.57	73.94	0.67	20.40	0.78	15.00
-86.41	39.32	US-MMS	5	0.67	89.27	0.70	53.94	0.73	17.00	0.87	12.16
-92.20	38.74	US-MOz	5	0.60	86.36	0.69	50.23	0.60	19.84	0.69	19.75
-82.24	29.76	US-SP2	5	0.27	160.04	0.25	36.50	0.74	21.01	0.61	20.95
-84.29	35.96	US-WBW	5	0.52	113.58	0.61	51.65	0.81	18.54	0.90	10.70
-98.48	55.88	CA-NS1	6	1.80	13.11	0.87	36.49	1.04	0.21	0.77	13.33
-98.52	55.91	CA-NS2	6	1.41	24.90	0.56	65.64	1.22	-1.71	0.85	11.07
-98.38	55.91	CA-NS3	6	1.65	17.76	0.77	47.40	1.10	-0.11	0.87	10.33
-98.38	55.91	CA-NS4	6	2.59	12.25	0.95	21.31	1.80	0.80	0.89	8.93
-98.49	55.86	CA-NS5	6	1.53	12.36	0.94	23.15	1.11	0.56	0.94	6.88
-99.95	56.64	CA-NS7	6	2.31	45.05	0.72	56.61	1.04	0.56	0.83	11.21
-121.95	45.82	US-Wrc	6	0.93	-7.75	0.81	34.30	0.82	2.63	0.64	14.71
-89.98	46.08	US-Los	7	0.74	98.07	0.52	75.02	0.93	9.90	0.89	11.06
-89.35	46.24	US-Syv	7	0.91	38.40	0.83	46.36	1.04	8.47	0.95	7.63
-90.08	45.81	US-WCr	7	0.78	54.64	0.75	59.25	0.90	12.99	0.90	10.85
-110.51	31.59	US-Aud	10	0.82	49.34	0.49	42.11	1.23	-2.36	0.70	18.77
-155.75	68.49	US-Ivo	10	1.65	9.08	0.57	27.83	0.80	7.20	0.62	10.14
-80.67	28.61	US-KS2	10	0.45	148.76	0.36	25.63	0.91	29.25	0.67	18.65
-116.64	33.38	US-SO4	10	1.32	37.85	0.31	42.54	0.35	18.28	0.07	20.30
-120.95	38.41	US-Var	10	0.62	59.95	0.72	32.77	0.65	16.55	0.75	10.18
-98.04	35.55	US-ARb	12	0.27	103.38	0.34	45.75	0.74	18.17	0.76	18.63
-98.04	35.55	US-ARc	12	0.32	98.57	0.32	46.30	0.68	17.94	0.71	20.22
-97.49	36.61	US-ARM	12	0.80	106.17	0.28	57.43	1.28	14.59	0.51	28.55
-96.84	44.35	US-Bkg	12	1.05	62.24	0.59	69.07	0.69	-2.61	0.77	19.17
-88.29	40.01	US-Bo1	12	0.33	123.55	0.26	88.55	0.81	6.18	0.82	14.56
-105.10	48.31	US-FPe	12	0.68	44.69	0.18	56.25	0.53	13.15	0.48	19.89
-93.09	44.71	US-Ro1	12	0.37	116.91	0.25	102.30	0.90	5.45	0.88	13.48
-93.09	44.72	US-Ro3	12	0.50	96.89	0.40	91.07	0.91	8.14	0.81	16.91
-109.94	31.74	US-Wkg	12	1.22	44.34	0.25	67.95	1.51	-3.65	0.51	26.96
-96.86	37.52	US-Wlr	12	0.78	86.50	0.65	47.84	0.99	6.83	0.72	22.56

Table 3 Comparison of model-derived forest carbon density (Mg C ha^{-1}) with those from other studies. Pan et al. (2001) calculated carbon densities for both above- and below-ground biomass. Numbers in brackets for Pan et al. (2011) show the AGB values assuming that the AGB accounts for 80% of total biomass density.

Source	Method	Forest Carbon Density (Mg C ha^{-1})			Carbon Stock (Pg)
		Europe	North America	Global	Global
Goodale et al.(2002)	Forest Inventary	38.8	44.6		
Liski et al.(2003)	Forest Inventary	43	43		
Thurner et al.(2014)	Remote Sensing	60.8±22.4	45.3±17.1		
Pan et al.(2011)	Forest Inventary	60.5 (48.4)	68.7 (54.9)	94.2 (75.4)	362.6 (290.1)
This Study	Model	59.24±20.04	53.74±36.39	82.96	276.5

Biogeosciences Discuss., doi:10.5194/bg-2016-142, 2016
Manuscript under review for journal Biogeosciences
Published: 25 April 2016

Figure captions

Fig. 1 Taylor diagram of (a) GPP (gC m^{-2} $year^{-1}$) and (b) ET (mm $year^{-1}$) for 39 flux towers.

Fig. 2 Comparison of annual observed and modeled values for (a) GPP (gC m^{-2} $year^{-1}$) and (b) ET (mm $year^{-1}$), and (c) independent validation of GPP on annual scale. The dashed line shows the 1:1 line.

Fig. 3 (a) Modeled GPP (gC m^{-2} $year^{-1}$) averaged for 2000–2011 and (b) difference between modeled value and that reported by Jung et al. (2011).

Fig. 4 (a) Modeled ET (mm $year^{-1}$) averaged for 2000–2011 and (b) difference between modeled value and that reported by Jung et al. (2011).

Fig. 5 Comparison of annual observed and modeled values for (a) site-year AGB (Mg ha^{-1}) and (b) different sites, and (c) independent validation. The dashed line shows the 1:1 line.

Fig. 6 (a) Modeled global patterns of AGB (Mg ha^{-1}) averaged for 2000–2010 and (b) latitudinal AGB patterns.

Biogeosciences Discuss., doi:10.5194/bg-2016-142, 2016
Manuscript under review for journal Biogeosciences
Published: 25 April 2016

Fig. 7 (a) Comparison of observed AGB (left panel, points show plot locations) and difference between modeled and observed AGBs for Amazonian forests (right panel), and (b) relative error [(Modeled − observed)/observed × 100%] frequency.

Fig. 8 (a) Difference between model-derived AGB driven by Princeton and CRU meteorological datasets. The Princeton and CRU data are on daily and monthly timescales, respectively.

Biogeosciences Discuss., doi:10.5194/bg-2016-142, 2016
Manuscript under review for journal Biogeosciences
Published: 25 April 2016

Figure 1

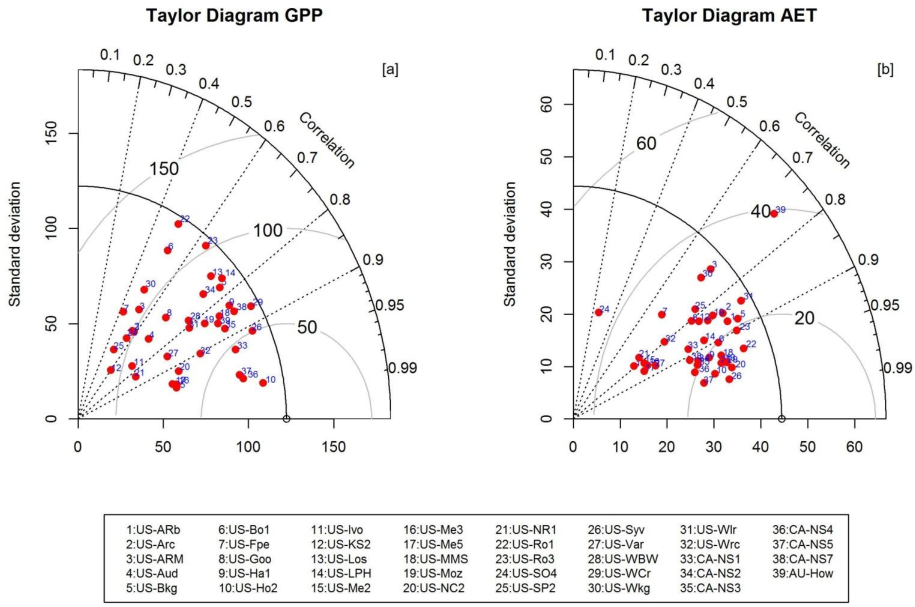

Biogeosciences Discuss., doi:10.5194/bg-2016-142, 2016
Manuscript under review for journal Biogeosciences
Published: 25 April 2016

664 **Figure 2**

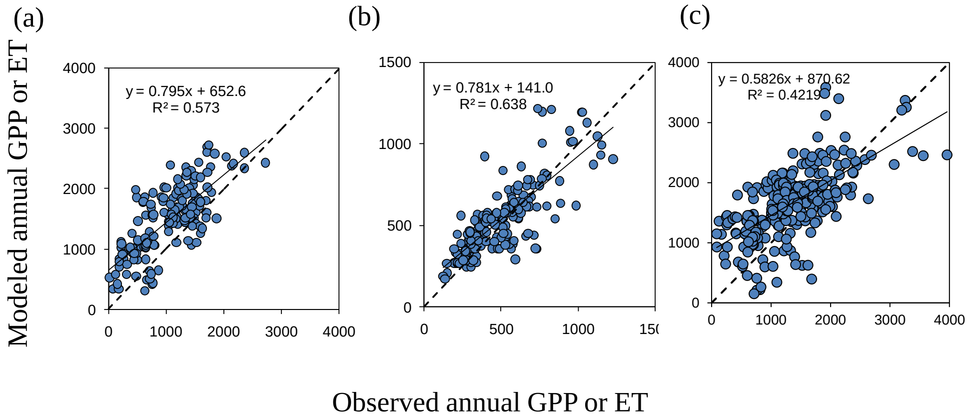

665

Biogeosciences Discuss., doi:10.5194/bg-2016-142, 2016
Manuscript under review for journal Biogeosciences
Published: 25 April 2016

Figure 3

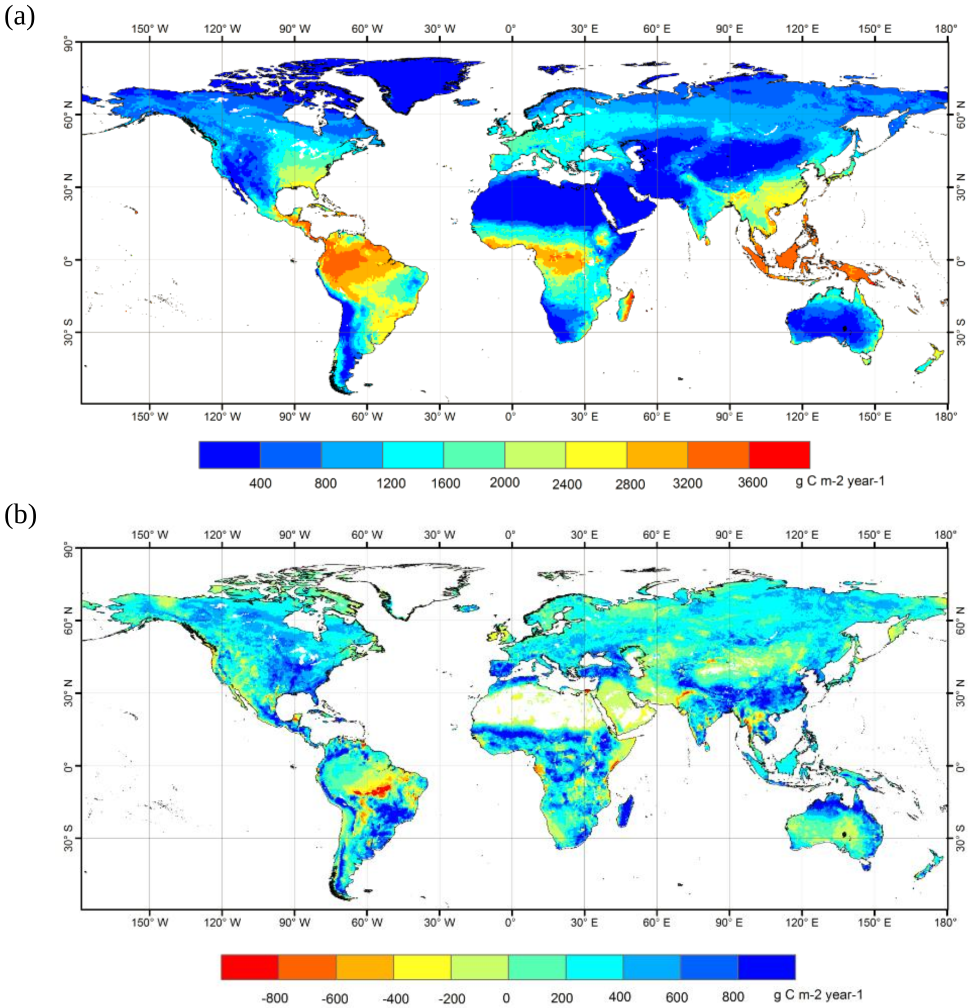

Biogeosciences Discuss., doi:10.5194/bg-2016-142, 2016
Manuscript under review for journal Biogeosciences
Published: 25 April 2016

Figure 4

(a)

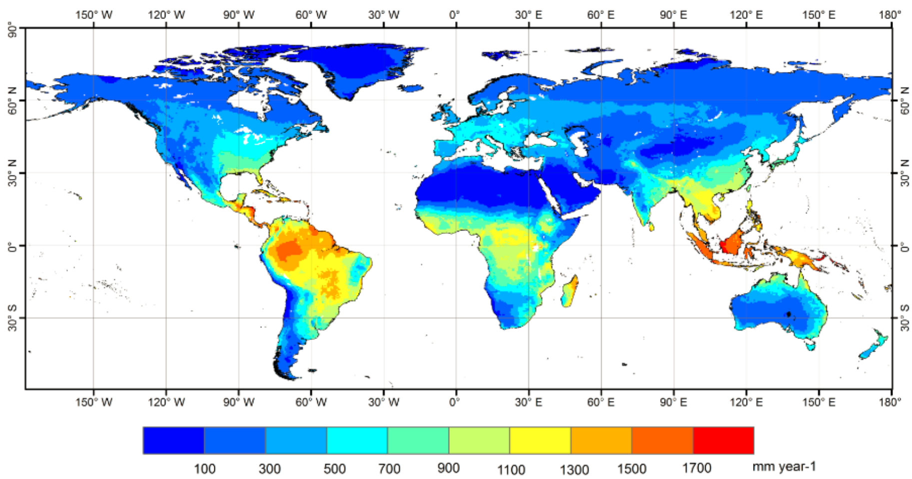

(b)

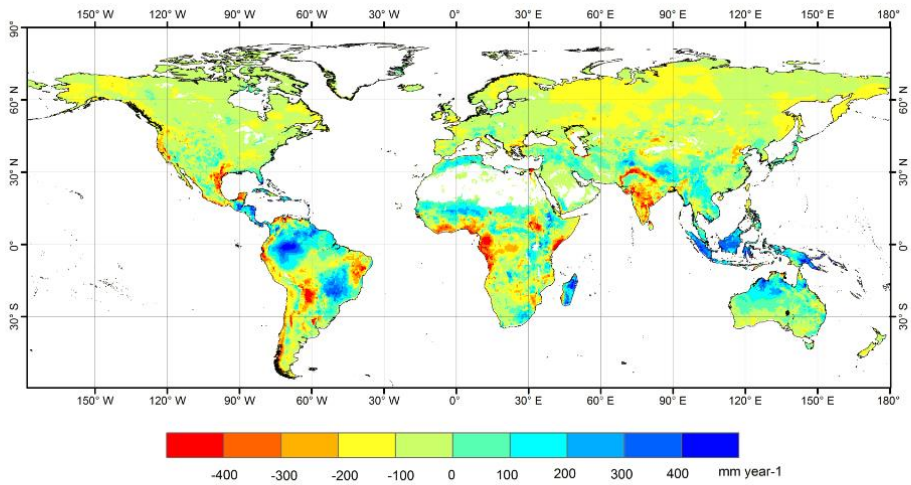

Biogeosciences Discuss., doi:10.5194/bg-2016-142, 2016
Manuscript under review for journal Biogeosciences
Published: 25 April 2016

Figure 5

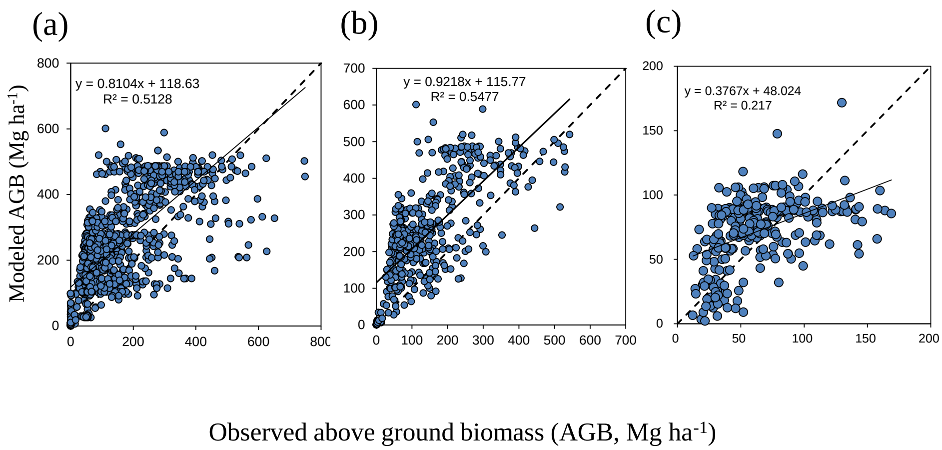

Biogeosciences Discuss., doi:10.5194/bg-2016-142, 2016
Manuscript under review for journal Biogeosciences
Published: 25 April 2016

673 **Figure 6**

(a)

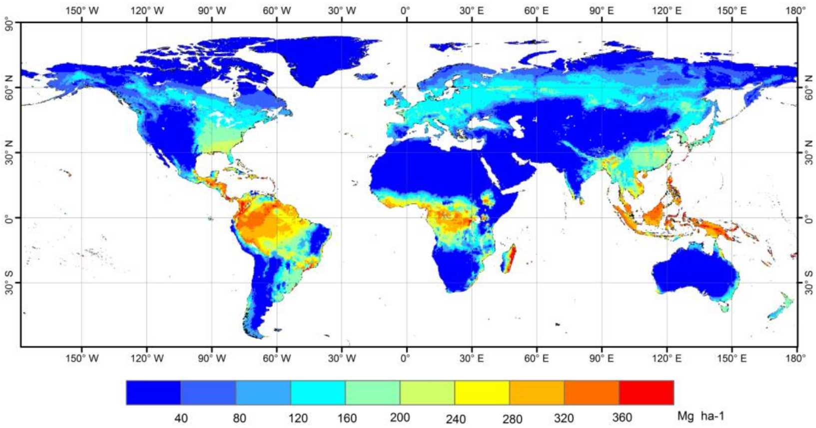

(b)

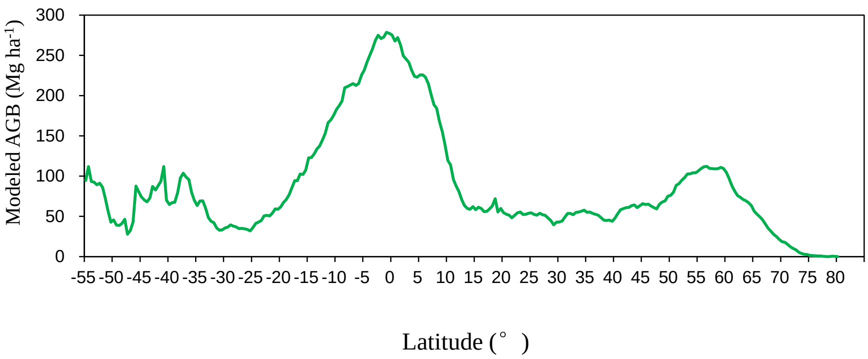

674

Biogeosciences Discuss., doi:10.5194/bg-2016-142, 2016
Manuscript under review for journal Biogeosciences
Published: 25 April 2016

Biogeosciences
Discussions
Open Access

Figure 7

(a)

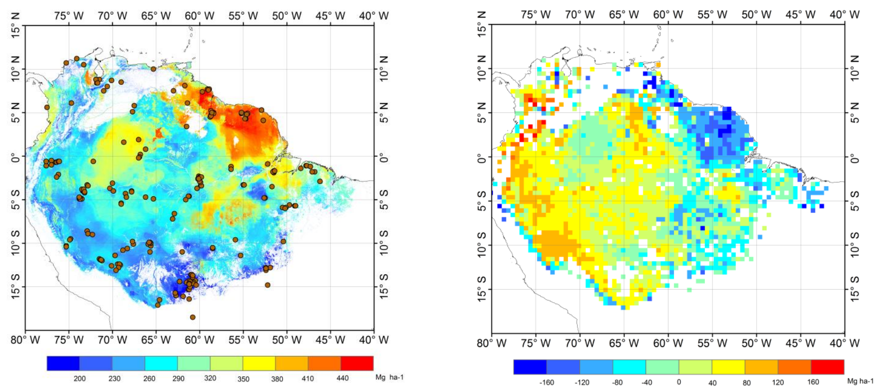

(b)

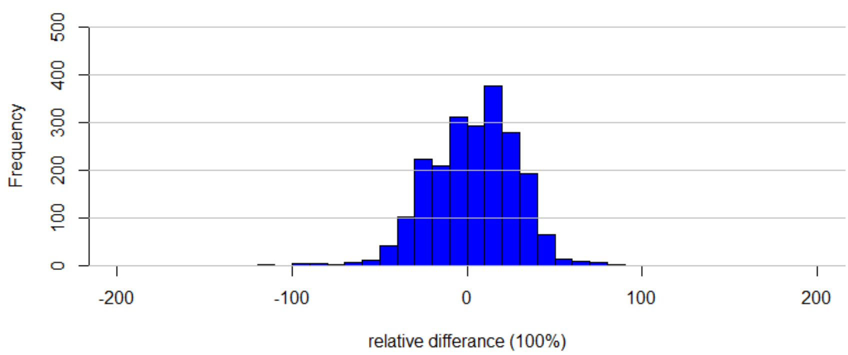

Biogeosciences Discuss., doi:10.5194/bg-2016-142, 2016
Manuscript under review for journal Biogeosciences
Published: 25 April 2016

Figure 8

(a)

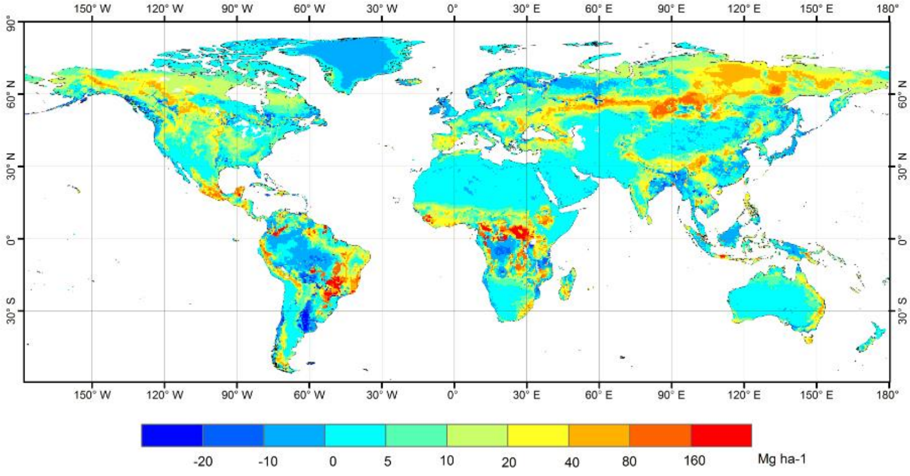

(b)